Cell

Regulation of Planar Cell Polarity by Smurf Ubiquitin Ligases

Masahiro Narimatsu,[1,5] Rohit Bose,[1,2,5] Melanie Pye,[1] Liang Zhang,[1] Bryan Miller,[3,4] Peter Ching,[3,4] Rui Sakuma,[1] Valbona Luga,[1,2] Luba Roncari,[1] Liliana Attisano,[3,4,*] and Jeffrey L. Wrana[1,2,*]

[1]Center for Systems Biology, Samuel Lunenfeld Research Institute, Mount Sinai Hospital, 600 University Avenue, Toronto, ON, Canada, M5G 1X5

[2]Department of Molecular Genetics

[3]Department of Biochemistry

[4]Donnelly Centre for Cellular and Biomolecular Research

University of Toronto, 160 College Street, Toronto, ON, Canada, M5S 3E1

[5]These authors contributed equally to this work

*Correspondence: liliana.attisano@utoronto.ca (L.A.), wrana@mshri.on.ca (J.L.W.)

DOI 10.1016/j.cell.2009.02.025

SUMMARY

Planar cell polarity (PCP) is critical for morphogenesis in metazoans. PCP in vertebrates regulates stereocilia alignment in neurosensory cells of the cochlea and closure of the neural tube through convergence and extension movements (CE). Noncanonical Wnt morphogens regulate PCP and CE in vertebrates, but the molecular mechanisms remain unclear. Smurfs are ubiquitin ligases that regulate signaling, cell polarity and motility through spatiotemporally restricted ubiquitination of diverse substrates. Here, we report an unexpected role for Smurfs in controlling PCP and CE. Mice mutant for *Smurf1* and *Smurf2* display PCP defects in the cochlea and CE defects that include a failure to close the neural tube. Further, we show that Smurfs engage in a noncanonical Wnt signaling pathway that targets the core PCP protein Prickle1 for ubiquitin-mediated degradation. Our work thus uncovers ubiquitin ligases in a mechanistic link between noncanonical Wnt signaling and PCP/CE.

INTRODUCTION

Planar cell polarity (PCP) refers to the phenomenon whereby cell polarity is coordinated within the plane of a tissue (Seifert and Mlodzik, 2007; Wang and Nathans, 2007; Zallen, 2007). In *Drosophila*, PCP operates at the tissue level to regulate the precise alignment of hairs and the hexagonal packing of wing epithelial cells, as well as the orientation of photoreceptors in the eye. In mammals, PCP is prominent in the alignment of stereocilia of the neurosensory hair cells of the cochlea (Lewis and Davies, 2002). A core group of conserved proteins including Van Gogh/Strabismus (Vang/Stbm or Vangl), Flamingo/Starry night/Cadherin EGF LAG seven-pass G-type receptor (Fmi/Stan/Celsr), Frizzled (Fz/Fzd), Dishevelled (Dsh/Dvl), Prickle (Pk), and Diego/Diversin play central roles in PCP (Seifert and Mlodzik, 2007; Wang and Nathans, 2007; Zallen, 2007) and mutations in *Celsr1*, *Vangl2*, *Dvl1/2*, and *Fz3/6* disrupt stereocilia orientation in mouse cochlea hair cells (Curtin et al., 2003; Montcouquiol et al., 2003; Wang et al., 2005, 2006b). Importantly, these mutants also display severe neural tube defects and a shortened anterior-posterior (AP) axis with concomitant expansion of the mediolateral axis (Curtin et al., 2003; Greene et al., 1998; Kibar et al., 2001; Montcouquiol et al., 2003; Murdoch et al., 2001; Wang et al., 2005, 2006a, 2006b). These problems reflect defective convergent extension (CE) movements, a process whereby axial mesoderm cells intercalate and converge toward the anterior-posterior (AP) axis (Keller, 2002; Wallingford et al., 2002). CE also occurs in the neurectoderm acting to narrow and elongate the neural floorplate thus enabling neural fold apposition and neural tube closure (Copp et al., 2003). The shared molecular basis of PCP and vertebrate CE demonstrates that PCP functions not only in establishment of organized epithelial sheets, but also in dynamic tissues to control directed cell migrations, polarized cell division and differentiation (Seifert and Mlodzik, 2007; Zallen, 2007).

PCP proteins are asymmetrically distributed in numerous contexts (Strutt, 2002). In the *Drosophila* wing, these components form discrete protein complexes that segregate to either the proximal (Vang and Pk), or distal (Fz, Dvl, and Diego) apical surface of cells. How asymmetric distribution is accomplished is not clear, though many PCP components, such as Dvl, Pk, Vangl and Diego physically interact (Bastock et al., 2003; Das et al., 2004; Jenny et al., 2005; Takeuchi et al., 2003; Torban et al., 2004; Tree et al., 2002). In vertebrates some PCP proteins are asymmetrically distributed in the inner ear, although species and cell-type differences in colocalization have been noted (Deans et al., 2007; Montcouquiol et al., 2006; Wang et al., 2005, 2006b). In dynamic tissues and motile cells, asymmetric distribution has not been well established and during CE in the mouse, Vangl2 and Dvl do not display asymmetry, though asymmetric Pk in the Ascidian notochord and the neural keel in Zebrafish was reported (Ciruna et al., 2006; Jiang et al., 2005). The extrinsic cues that regulate PCP and CE at both the local and tissue level have remained obscure. However, Fzds and Dvl, which are core PCP proteins, are also key Wnt signaling

components (Wang and Nathans, 2007) and while Wnt ligands are not required for PCP in *Drosophila*, in vertebrates, noncanonical Wnt ligands are important regulators of PCP/CE (Qian et al., 2007; Seifert and Mlodzik, 2007; Wang and Nathans, 2007; Zallen, 2007). Furthermore, the polarity protein, Par6, has been shown to play an important role in controlling stabilized cell protrusions during CE in the frog (Hyodo-Miura et al., 2006). The relationship between noncanonical Wnt, PCP, CE and/or asymmetric PCP protein localization remains enigmatic.

Smurf1 (Smad ubiquitination regulatory factor-1) and Smurf2 are related E3 ubiquitin ligases of the C2-WW-HECT class that play a key roles in regulating signaling, cell polarity and motility (Izzi and Attisano, 2006). In particular, Smurfs function as effectors of the polarity protein Par6 to regulate cell motility and polarity by local targeting of RhoA for degradation (Sahai et al., 2007; Wang et al., 2003) and during epithelial-to-mesenchymal transition (EMT) TGFβ-dependent recruitment of Smurf to Par6 mediates dissolution of tight junctions (Ozdamar et al., 2005). Here, we show that mutation of *Smurf1* and *Smurf2* in the mouse leads to PCP and CE defects and that Smurfs act in a noncanonical Wnt pathway as effectors of a Par6-Dishevelled complex that targets Prickle1 for ubiquitin-mediated degradation. These results thus demonstrate that Smurf ubiquitin ligases function in noncanonical Wnt signaling to regulate core PCP pathway components.

RESULTS

Mouse Embryos Lacking Smurf1 and Smurf2 Display CE and Neural Tube Defects

To explore the role of Smurfs in vivo, we generated *Smurf1*$^{-/-}$ and *Smurf2*$^{-/-}$ mice by disrupting the genes through targeted homologous recombination (Figure S1). Individual *Smurf1*$^{-/-}$ and *Smurf2*$^{-/-}$ mice were viable, fertile and were born at the expected Mendelian ratios, indicating no overt defects in embryogenesis (data not shown), as previously reported for *Smurf1*$^{-/-}$ mice (Yamashita et al., 2005). The similar expression patterns observed for *Smurf1* and *Smurf2* (Figure S2) likely provides for redundancy. We therefore generated mice lacking both *Smurf1* and *Smurf2*. No double knockout *Smurf1*$^{-/-}$;*Smurf2*$^{-/-}$ (*Smurf* DKO) embryos were born with most dying around embryonic day E10.5 and none recovered beyond E12.5 (see Table S1 available with this article online). *Smurf* mutants displayed two distinct phenotypes. Type I mutants (approximately 35% of DKO embryos) displayed gastrulation defects characterized by abnormal posterior structures (M.N., M.P. and J.L.W., unpublished data) and will be described elsewhere. In contrast, type II mutants gastrulated normally, but by the 6 somite stage displayed gross morphological aberrations that included a completely open neural tube (Figure 1A). Neural tube closure occurs at this stage with a process termed closure 1 that initiates when the neuroepithelium bends at the floor plate to form the median hinge point (MHP) (Copp et al., 2003). Mutant embryos with lateral expansion of the neural plate and in particular the floor plate, typically fail in closure 1. Analysis of transverse sections of E8.75 *Smurf* DKO mutants indeed revealed that the neuroectoderm was splayed open with ectopic invaginations and an expanded floorplate (Figure 1A, black arrow). *Smurf* mutant embryos thus fail at closure 1 due to lateral expansion of the neuroectoderm and severe broadening of the floor plate.

In addition to the MHP, formation of dorso-lateral hinge points (DLHPs) is also required for closure of the neural tube at the caudal regions at a later stage (Copp et al., 2003). BMPs inhibit DLHP formation (Ybot-Gonzalez et al., 2007), raising the possibility that loss of Smurfs, which inhibit BMP signaling, might block neural tube closure by enhancing BMP signaling. However, the caudal region of *Smurf* DKO embryos formed DLHPs, despite the lateral expansion of the neural plate (Figure 1A). Moreover, both WT and *Smurf* DKO embryos displayed similar dorso-ventral (DV) gradients of phospho-Smad1 (Figure S3). Thus the neural tube defects of *Smurf* DKO embryos are unlikely to reflect hyperactivation of BMP signaling.

A completely open neural tube, termed craniorachischisis, accompanied by a broadened neural floorplate is characteristic of PCP pathway mutants including *Dvl1/2 and Vangl2* (Greene et al., 1998; Wang et al., 2006a) and is thought to be the result of defective CE movements. Since CE narrows the medial-lateral dimension (width) while extending the anterior-posterior (AP) axis (length), we analyzed the aspect ratio of *Smurf* DKO embryos. This revealed significant shortening of the AP axis and concomitant increase in width (Figure 1B). Furthermore, analysis of *Brachyury*, a marker of the axial mesoderm and primitive streak, revealed a broadened expression domain in the notochord of *Smurf* E8.0 DKO embryos (Figure 1C). Lateral expansion of *Sonic hedgehog* (*Shh*) expression, which marks the notochord, was also evident in *Smurf* DKO embryos, particularly at the posterior end (Figure 1D). To better understand the defects underlying the expanded neural plate and axial mesoderm, we analyzed expression of Foxa2 (HNF3β), a marker of the floorplate, axial mesoderm and definitive endoderm. This revealed that Foxa2-expressing floor plate cells were spread laterally at the mid-trunk region and the posterior end of *Smurf* DKO embryos when compared to controls (Figure 1E) and that the floorplate of *Smurf* DKO embryos was either flat at the posterior region, or a U-shaped at the mid-trunk region. Furthermore, mixing of non-Foxa2-expressing cells could clearly be detected in the mutant floorplates. Thus, *Smurf* DKO mice display severe CE defects that include reduced axial elongation and a broadened midline along with a completely open neural tube and a broadened neural floorplate and axial mesoderm. These defects are remarkably similar to those observed in mutants of known PCP pathway components suggesting that Smurfs function in this pathway.

Smurf1$^{-/-}$;*Smurf2*$^{+/-}$ and *Smurf1*$^{+/-}$;*Smurf2*$^{-/-}$ Mice Display CE Defects

PCP mutant mice, which harbour severe neural tube closure defects, concomitantly display disruptions in the inner ear (Lewis and Davies, 2002). *Smurf* DKO embryos do not survive past E12.5. To reduce the severity of the defects, we generated mice lacking three of the four *Smurf* alleles (ie *Smurf1*$^{-/-}$;*Smurf2*$^{+/-}$ and *Smurf1*$^{+/-}$;*Smurf2*$^{-/-}$). The birth rate of *Smurf1*$^{-/-}$;*Smurf2*$^{+/-}$ and *Smurf1*$^{+/-}$;*Smurf2*$^{-/-}$ mice was less than the expected Mendelian ratio (Table S2) and at E14.5, 25% of either *Smurf1*$^{-/-}$;*Smurf2*$^{+/-}$ or *Smurf1*$^{+/-}$;*Smurf2*$^{-/-}$ embryos displayed neural tube defects (NTD) that were of

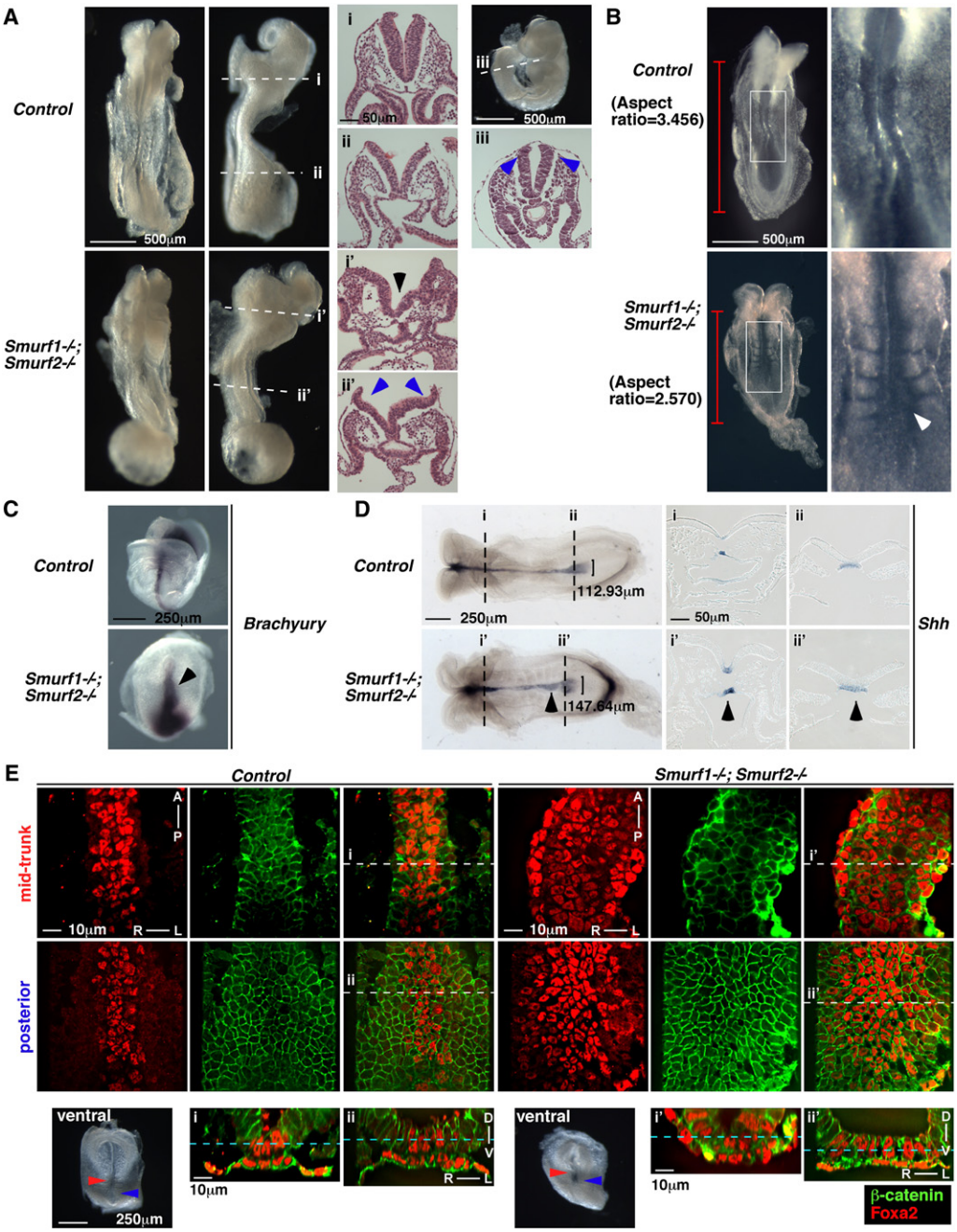

Figure 1. *Smurf* DKO Mutants Exhibit Severe Convergent Extension Defects

(A) Dorsal and lateral view of double homozygous *Smurf* DKO mutants around E8.5 to 8.75. Broken lines indicate the positions of H&E stained transverse sections. *Smurf* mutants show disorganized neuroectoderm and lateral expansion of the floor plate (black arrowhead). Formation of dorso-lateral hinge points (blue arrowheads) is maintained in *Smurf* DKO mutants.

(B) *Smurf* DKO mutant shows a short A-P axis and laterally expanded body (left). Lateral expansion of the floor plate is evident (white arrowhead) in higher magnification images (right).

(C and D) Expression of *Brachyury* and *Sonic hedgehog (Shh)* in *Smurf* DKO mutants. *Brachyury* expression in the notochord is wider and more diffuse at E8.0. Expression of *Shh* is maintained but the notochord shows lateral expansion (arrowheads). The node width (in μm) is indicated (left).

(E) Lateral expansion of the floorplate in *Smurf* DKO mutants. Optical sections of the E8.0 floorplate from embryos immunostained with anti-Foxa2 and β-catenin are shown (top and middle rows). Ventral images of the embryos and 3D-reconstructed transverse sections are shown (bottom). Note that the second layer of cells that are basal to the neural tube in *Smurf* DKO mutants are laterally expanded axial mesendoderm. White dashed lines indicate AP positions of the reconstructed transverse sections and blue dashed lines indicate DV positions of the optical sections. Blue/red arrowheads on the whole mount images show positions scanned. AP, DV and right-left (RL) axes are indicated.

reduced severity compared to *Smurf* DKOs and included exencephaly and spina bifida (Figure S4A and Table S3). In addition, we occasionally observed *Smurf1*$^{-/-}$;*Smurf2*$^{+/-}$ and *Smurf1*$^{+/-}$;*Smurf2*$^{-/-}$ embryos with a looped tail (Figure S4A), similar to that observed in mutants for PCP pathway components such as *Vangl2* and *Celsr1* (Curtin et al., 2003; Greene et al., 1998). Analysis of transverse sections of earlier 5 and 6 somite stage embryos (Figure S4B) revealed that *Smurf1*$^{+/-}$;*Smurf2*$^{-/-}$ embryos showed a delay in bending at the MHP (Figures S4Bi'' and S4Bii''). Furthermore, lateral expansion of the posterior notochord was observed in *Smurf1*$^{+/-}$;*Smurf2*$^{-/-}$ at 5 and 6 somite stages (Figure S4D), as well as reduced length-to-width ratios (Figure S4C). Consistent with CE defects, in situ hybridization analysis revealed lateral expansion of *Foxa2* expression in *Smurf1*$^{+/-}$;*Smurf2*$^{-/-}$ embryos (Figure S4D). In contrast, *Smurf1*$^{-/-}$; *Smurf2*$^{+/-}$ embryos were indistinguishable from wild-type mice. Of note, by the 7 and 8 somite stages the length-to-width ratio of *Smurf1*$^{+/-}$;*Smurf2*$^{-/-}$ mutants was similar to WT controls (data not shown). Overall, these results demonstrate that while *Smurf* DKO animals display severe CE defects, introduction of one copy of either *Smurf1* or *Smurf2* can rescue the phenotype. Of note, *Smurf1*$^{+/-}$;*Smurf2*$^{-/-}$ embryos displayed a delay in AP axis elongation, suggesting that Smurf2 may be more important at this stage of development than Smurf1.

Misorientation and Disorganization of Sensory Hair Cells in *Smurf1*$^{-/-}$;*Smurf2*$^{+/-}$ and *Smurf1*$^{+/-}$;*Smurf2*$^{-/-}$ Cochlea

We next examined the cochlea of E18.5 *Smurf1*$^{-/-}$;*Smurf2*$^{+/-}$ and *Smurf1*$^{+/-}$;*Smurf2*$^{-/-}$ mice for PCP defects in the organ of Corti. No significant difference in the gross appearance of the cochlea between control and embryos lacking either combination of 3 *Smurf* alleles was observed. However, examination of the apical surface of the organ of Corti near the basal region by immunostaining and confocal scanning microscopy revealed that in wild-type mice, the stereocilia (stained red with phalloidin) were aligned in a well organized "chevron" formation in relation to the single kinocilium per cell (Figure 2A; stained yellow with anti-acetylated tubulin). In contrast, in both *Smurf1*$^{-/-}$;*Smurf2*$^{+/-}$ and *Smurf1*$^{+/-}$;*Smurf2*$^{-/-}$ mice, the stereocilia bundles were misaligned (Figure 2A; white arrowheads). Misorientation of cells was most pronounced in the outer hair cell (OHC) layers with mispositioning of cells (green arrowheads) also observed. While these defects are comparable in severity to *Dvl1/2* or *Fzd3/6* double deficient mutants, they are not as severe as those observed in embryos null for *Vangl2* or *Celsr1* (Curtin et al., 2003; Montcouquiol et al., 2003; Wang et al., 2006a, 2006b). This likely reflects the presence of one wild-type *Smurf* allele in these mutants.

To further examine OHC morphology, images from the apical to basal layers were collected by confocal microscopy (Figure 2B). This revealed that misoriented OHC, evident on the apical surface (Figures 2A and 2B), were also observed basally in compound *Smurf* mutants. In particular, at the basal layer of wild-type mice, the OHC displayed a highly organized arrangement in a hexagonal pattern (Figure 2B), reminiscent of the epithelium of pupal fly wings. However, OHC from *Smurf1*$^{-/-}$;*Smurf2*$^{+/-}$ and *Smurf1*$^{+/-}$;*Smurf2*$^{-/-}$ often displayed abnormal cell shape and cell-cell contacts, resulting in the appearance of pentagonal or heptagonal shaped cells (Figure 2B). Although not previously reported in other PCP mutant mice, defects in the hexagonal arrangement of cells have been observed in the wing of *Drosophila* PCP mutants (Classen et al., 2005). How hexagonal packing of OHCs is disturbed in *Smurf* mutants is unclear but may reflect a failure to remodel tight junctions during tissue morphogenesis. Taken together, these results demonstrate that Smurfs play a role in the establishment or maintenance of PCP in the inner ear, including the orientation of the hair cells and cell contacts.

Smurf1 and Smurf2 Interact with Phosphorylated Dvl2

Our analysis of *Smurf* mutants indicated that Smurfs function to regulate CE and PCP pathways that are linked to noncanonical Wnt signaling. Therefore we sought to identify Smurf binding partners in the Wnt pathway using LUMIER, a mammalian cell-based protein-protein interaction approach (Barrios-Rodiles et al., 2005). Renilla luciferase-tagged catalytically inactive C716A (CA) Smurf2 was expressed in human embryonic kidney (HEK) 293T cells together with individual Flag-tagged proteins comprised of a set of 99 implicated or known components of the Wnt signaling network (Table S4). Protein interactions were examined by performing a Renilla luciferase enzymatic assay on anti-Flag immunoprecipitates. This revealed that Smurf2 associated with Dvls 1, 2, and 3 (Figure 3A), which are core PCP components and essential mediators of both noncanonical and canonical Wnt signaling. Verification by immunoprecipitation and immunoblotting also showed that interactions with Dvl2 were independent of Smurf ubiquitin ligase activity (Figures 3 and S5A and data not shown) and that the interaction was reduced but not abrogated by deletion of either the Dvl2 PY motif (Figure S5B) or the Smurf2 WW2 domain (Figure S5C). PY motif-WW domain interactions thus drive Dvl2-Smurf interactions with additional surfaces contributing to the interaction as observed for other Smurf partners (Ogunjimi et al., 2005).

Activation of the Wnt pathway by overexpressing the Wnt receptor, Frizzled7 (Fzd7) significantly enhanced Smurf1 and Smurf2 interaction with Dvl2 (Figure 3B). Wnt signaling induces phosphorylation of Dvls, visualized by an upward mobility shift upon SDS-PAGE analysis (Figure 3C). Phosphorylated Dvls are also easily detected upon overexpression, likely due to saturation of inhibitory pathways. Interestingly, Dvl2 bound to Myc-Smurf2 was the slower migrating form (Dvl2*; Figure 3C) that was converted to the more rapidly migrating form by phosphatase treatment (Figure 3D). This suggests that Smurf2 preferentially associates with phosphorylated Dvl2. Dvl phosphorylation sites have not yet been defined, but through a fortuitous PCR mutation we identified a nonphosphorylated point mutant of Dvl2 that is comprised of a Glu 499 to Gly mutation (Dvl2EG) located in a loop between the antiparallel β strands at the carboxyl-terminus of the DEP domain. Phosphatase treatment confirmed loss of phosphorylation (Figure S6A), while interaction of Dvl2(EG) with the known partners, Pak1, Nkd1, CK2 and Dab2 were maintained (data not shown), demonstrating that this mutant retains overall structural integrity. In contrast, Smurf2

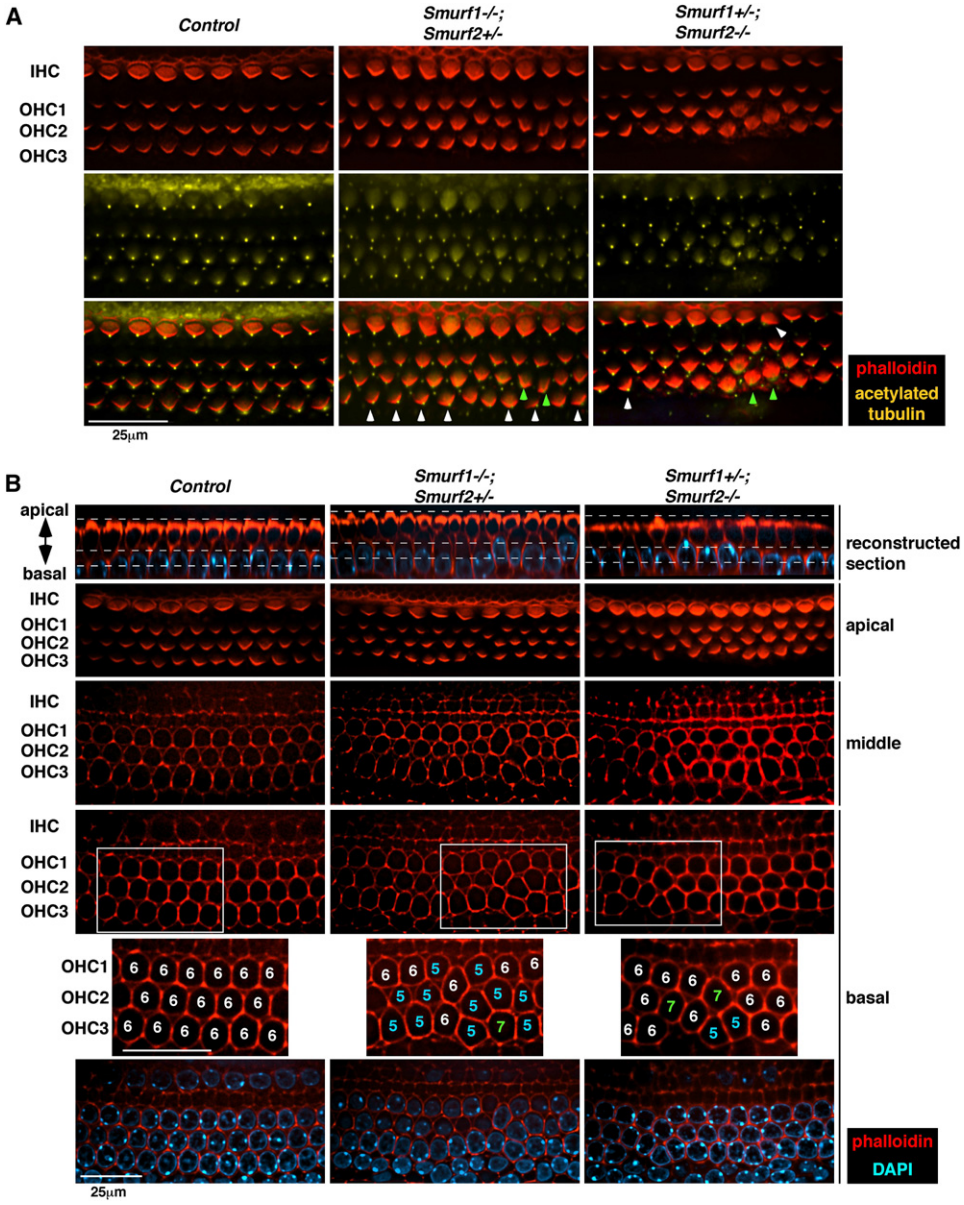

Figure 2. *Smurf* Mutants Lacking Three Alleles Show Disorganization of Cell Morphology/Cell-Cell Contact in Sensory Epithelial Cells of the Organ of Corti

(A) Apical surface of the organ of Corti. The sensory cilia bundles stained with phalloidin (red) and kinocilia stained with anti-acetylated tubulin antibodies (yellow) show misorientation (white arrowheads) and mispositioning (green arrowheads) of inner ear hair cells.

(B) 3D-reconstructed images (longitudinal sections along the OHC2 row) and optical sections at an apical, middle, and basal layer stained with phalloidin (red) are shown. Dashed lines indicate positions of optical sections. Cell-cell contact and cell shape at a middle/basal position is disorganized in *Smurf* mutants. High-magnification images of the indicated area with the number of edges for each polygonal shaped cell is shown. IHC; inner hair cells, OHC 1-3; outer hair cells 1-3. The scale bars represent 25 μm.

failed to associate with Dvl2(EG) (Figure 3E). Smurfs thus interact specifically with phosphorylated, activated Dvls.

The DEP domain is important for PCP signaling (Axelrod et al., 1998; Boutros et al., 1998) and a *Drosophila* PCP-specific mutant in a conserved cysteine residue (A21; C472R) has been identified in the same loop where the E499G mutation is located (Penton et al., 2002). Therefore, we also tested interaction of Smurf2 with the corresponding PCP mutant of Dvl2 (Figure S6A). This revealed that Dvl2(C501R) interacted poorly with Smurf2 (Figure S6C) despite efficiently activating canonical Wnt signaling (Figure S6D). Disruption of Dvl2-Smurf2 interactions by a PCP-specific mutation in the DEP domain supports the notion that the Dvl/Smurf interaction functions in noncanonical Wnt signaling.

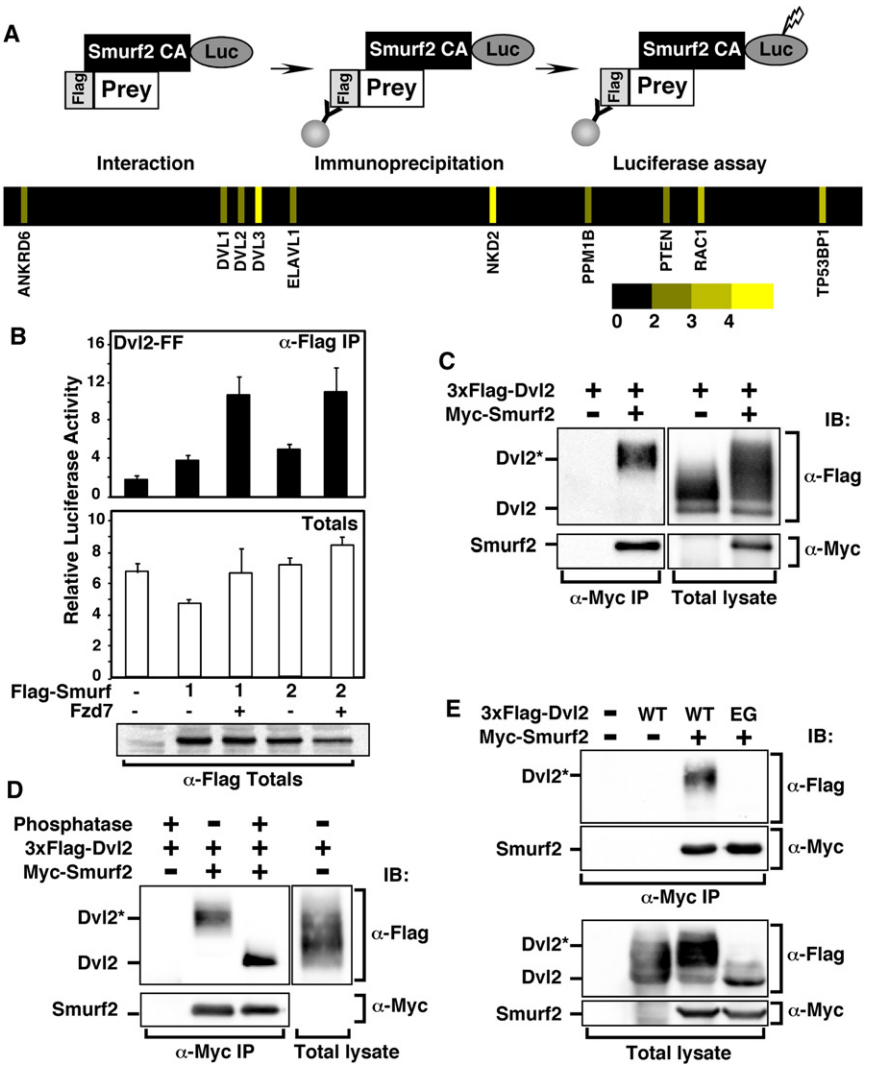

Figure 3. Smurf2 Interacts Specifically with Phosphorylated Dvl2

(A) Detection of Smurf2 interacting proteins using the LUMIER assay. The interaction of Luciferase-tagged catalytically-inactive C716A Smurf2 (Smurf2 CA-Luc) with individual Flag-tagged proteins assessed by luciferase assay. Each of the 99 Flag-tagged protein tested in the screen is represented as a vertical bar and the luminescence intensity ratio (LIR), which reflects the intensity of the interaction with Smurf2 is represented by the yellow tone, as indicated on the scale. Proteins displaying significant interactions are listed.

(B) Activation of the Wnt pathway enhances the interaction between Smurf and Dvl2. HEK293T cells were transfected with Firefly luciferase (FF)-tagged Dvl2 together with either Flag-Smurf1 CA or Smurf2 CA in the absence or presence of Fzd7. Dvl2 interaction with Smurf was determined by measuring FF activity in anti-Flag immunoprecipitates. The data represent mean of three samples ± SD.

(C and D) Smurf2 interacts with phosphorylated Dvl2. Lysates from HEK293T cells transfected with Myc-Smurf2 CA and 3xFlag-Dvl2 were subjected to anti-Myc Smurf2 immunoprecipitation (IP) directly followed by anti-Flag Dvl2 immunoblotting (IB) (C) or incubated in the presence or absence of alkaline phosphatase (D), followed by anti-Flag IB.

(E) A nonphosphorylatable point mutant of Dvl2 fails to interact with Smurf2. Lysates from HEK293T cells transfected with Myc-Smurf2 CA and WT or a nonphosphorylatable point mutant of 3xFlag-Dvl2 (EG), were subjected to anti-Myc Smurf2 IP and anti-Flag Dvl2 IB.

Noncanonical Wnt5A and Dvl2 Mediate the Assembly of the Smurf-Par6 Polarity Complex

We previously showed that Smurfs regulate both cellular protrusive activity and apico-basal polarity via interactions with the Par6 polarity network (Barrios-Rodiles et al., 2005; Ozdamar et al., 2005; Wang et al., 2003). Analysis of a LUMIER-based high-throughput screen of the Wnt pathway revealed an association of Par6 with all three Luciferase tagged Dvls, Dvl1, 2, and 3 (B.M. and L.A, unpublished data). Consequently, we examined the relationship between Par6, Dvl2 and Smurf. Unlike Smurf2, Par6 interacted with both Dvl2 WT and the phosphorylation mutant Dvl2(EG) (Figure 4A, left panel). Domain mapping by LUMIER revealed that the interaction required the region in Dvl2 between the DIX and PDZ domains (Figure S7A). We next examined whether Dvl2 might recruit Smurf2 to Par6. For this, a portion of lysates from cells expressing different combinations of Par6, Dvl2, Dvl2(EG) and Smurf2, were subjected to anti-Myc Smurf2 immunoprecipitation followed by anti-HA Par6 immunoblotting (Figure 4A, right). This revealed that Par6-Smurf2 association required co-expression of wild-type Dvl2, while Dvl2(EG) did not support this interaction, despite interacting with Par6. Analysis of Smurf1 revealed a similar Dvl2-dependent association with Par6 (Figure S7B).

We next examined the association of endogenous Par6, Dvl2 and Smurfs in the presence of the noncanonical Wnt ligand, Wnt5A, using MDA-MB-231 human mammary carcinoma cells. Endogenous Par6 interacted with Dvl2 irrespective of the presence or absence of Wnt5A (Figure 4B). In contrast, the interaction of endogenous Smurf2 with Par6 required Wnt5A stimulation. As Wnt5A induced Dvl phosphorylation (Figure 4B), this is consistent with the observation that phosphorylated Dvl2 recruits Smurfs into a tripartite complex with Par6 (Figure 4A). To confirm this, lysates from HEK293T cells expressing Flag-Dvl2, HA-Par6C and Myc-Smurf2 were subjected to anti-Flag immunoprecipitation, followed by Flag-peptide elution, anti-Myc immunoprecipitation and then anti-HA immunoblotting. This two-step procedure confirmed that Par6, phosphorylated Dvl2 and Smurf2 form a tri-protein complex (Figure 4C). As expected, Dvl2(EG), which prevents Smurf2 recruitment, blocked formation of the complex. Finally, we mapped the region of

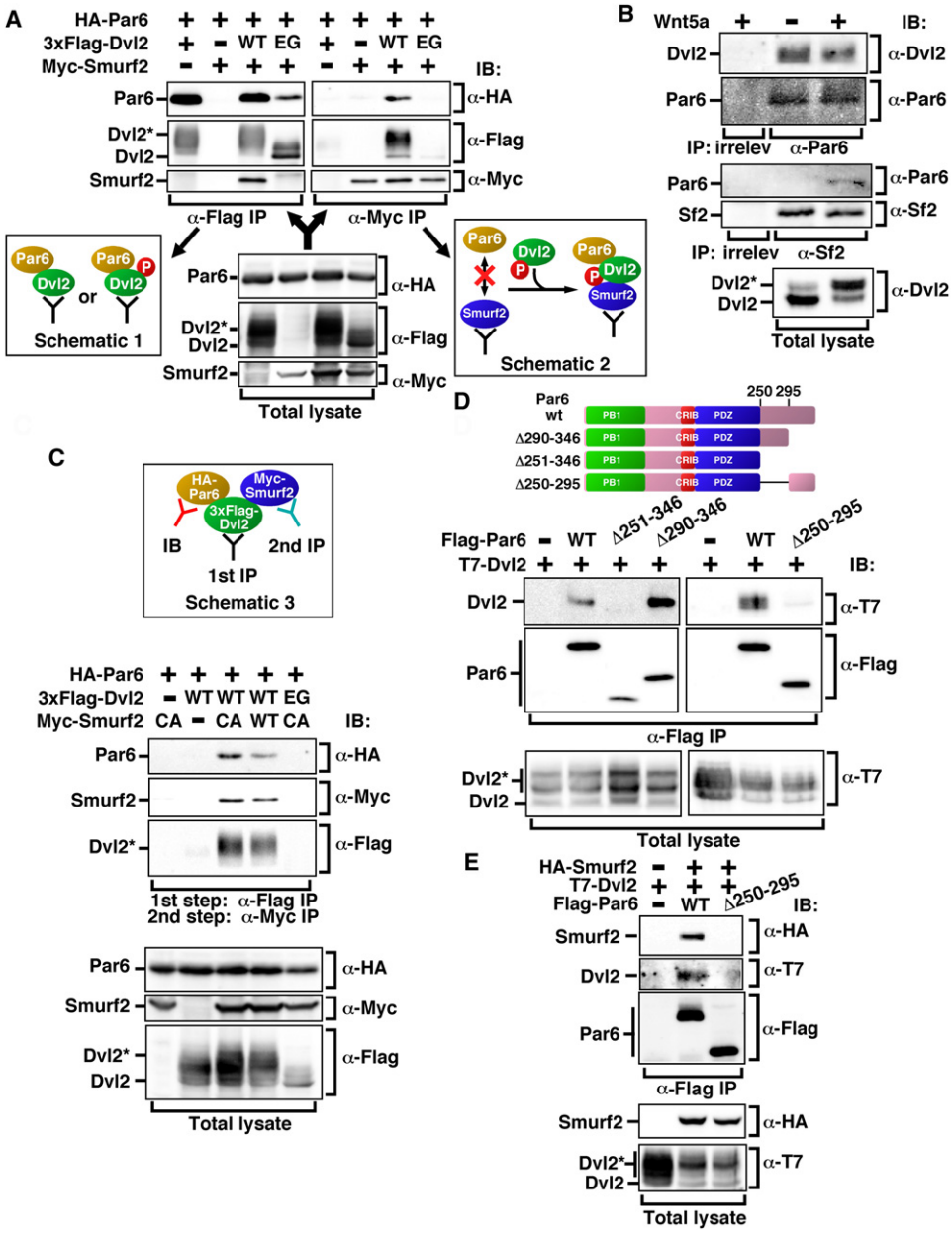

Figure 4. Noncanonical Wnt5A and Dvl2 Mediate the Assembly of the Smurf-Par6 Polarity Complex

(A) Par6 interacts constitutively with Dvl2, and requires Dvl2 for interaction with Smurf2. HEK293T cells were transfected with HA-Par6, Myc-Smurf2 and wild-type (WT) or the nonphosphorylatable point mutant (EG) of 3xFlag-Dvl2. The lysate was split and subjected either to anti-Flag Dvl2 immunoprecipitation (IP) with anti-HA Par6 immunoblotting (IB) (left side) or anti-Myc Smurf2 IP with subsequent anti-HA Par6 IB (right side).

(B) Wnt5A induces recruitment of Smurf2 to Par6. MDA-MB-231 human mammary carcinoma cells were incubated for 4h in the absence or presence of Wnt5A. The lysate was split and subjected to anti-Smurf2 (Sf2) IP and anti-Par6 IB (top panel) or anti-Par6 IP and anti-Dvl2 IB (middle panel).

(C) Par6, Dvl2* and Smurf2 form a heterotrimeric complex. Lysates from HEK293T cells transfected with HA-Par6, Myc-Smurf2 and WT or EG version of 3xFlag-Dvl2 were subjected to an anti-Flag Dvl2 IP, Flag-peptide elution, anti-Myc Smurf2 IP and then anti-HA Par6 IB.

(D and E) Par6 requires a region adjacent to PDZ domain for interaction with Dvl2 and Smurf2 binding. Lysates from HEK293T cells transfected with the indicated combinations of WT or truncation mutants of Flag-tagged Par6, T7-Dvl2 and HA-Smurf2 CA were subjected to anti-Flag Par6 IP followed by anti-T7 Dvl2 or anti-HA-Smurf2 IB.

Par6 required for Dvl2 association to a region adjacent to the Par6 PDZ domain, between residues 251 and 290 (Δ250–295) (Figure 4D). This deletion does not disrupt the tertiary structure of the adjacent PDZ domain, as Par6(Δ250–295) retained PDZ-dependent interactions with Par3 (Figure S7C). However, the Par6(Δ250–295) mutant was unable to bind Smurf2 in the

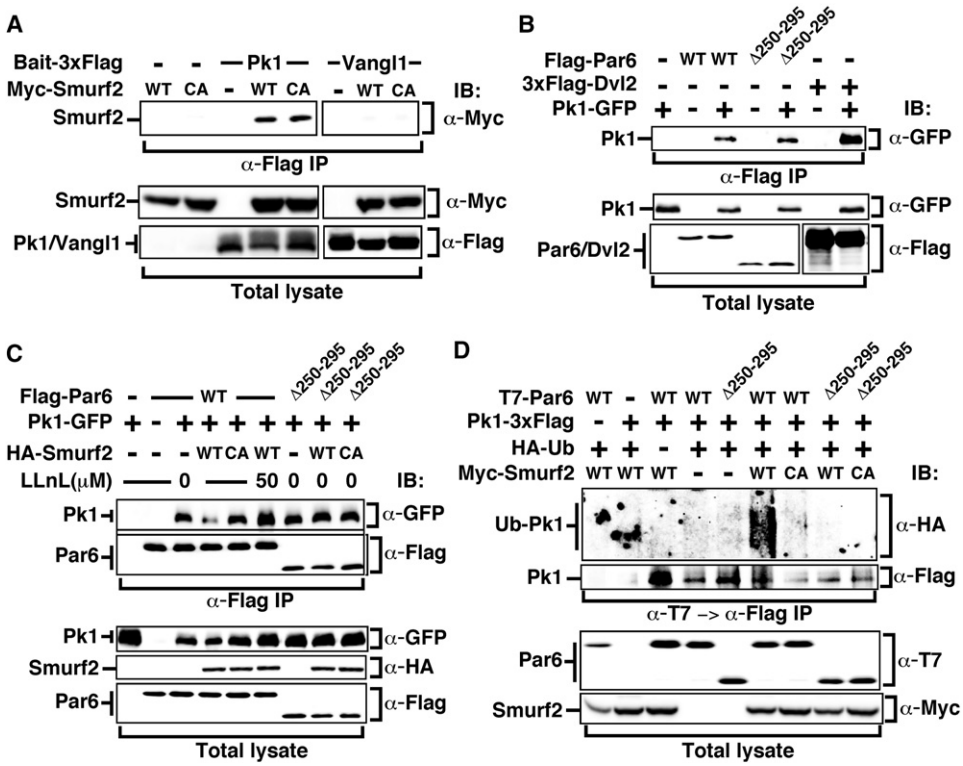

Figure 5. Smurf2 and Par6 regulate Prickle1 Turnover through the Ubiquitin-Proteasome Pathway

(A) Prickle1, but not Vangl1, physically interacts with Smurf2. Cell lysates from HEK293T cells transfected with Pk1-3xFlag, Vangl1-3xFlag and WT or catalytically inactive (CA) Myc-Smurf2 were subjected to anti-Flag immunoprecipitation (IP) and anti-Myc immunoblot (IB).

(B) Prickle1 physically interacts with Par6 and Dvl2. Cell lysates from HEK293T cells transfected with Pk1-GFP, Dvl2-3xFlag, and WT or the Dvl2-binding mutant (Δ250–295) of Flag-Par6 were subjected to anti-Flag IP and anti-GFP IB.

(C) Smurf2 decreases the level of Par6-bound Prickle1 in a proteasome-dependent manner. HEK293T cells were transfected with Pk1-GFP, Flag-Par6, Flag-Par6(Δ250–295), HA-Smurf2 and HA-Smurf2 CA. Cells were treated for 16 hr with 50 μM LLnL prior to lysis and anti-Flag IP.

(D) Ubiquitination of Par6-bound Prickle1 by Smurf2. HEK293T cells were transfected with T7-Par6 and T7-Par6(Δ250–295), Pk1-3xFlag, HA-ubiquitin, Myc-Smurf2 and Myc-Smurf2 CA. Cells were treated for 16 hr with or without 50 μM LLnL prior to lysis and anti-T7 IP (1st IP). The precipitates were eluted by boiling in 1% SDS and then subjected to anti-Flag IP (2nd IP).

presence of Dvl2 (Figure 4E). Altogether, these data demonstrate that Dvl2 and Par6 can associate constitutively and suggest a model in which Wnt5A induced Dvl2 phosphorylation mediates recruitment of Smurfs to the polarity protein, Par6.

The Par6-Dvl-Smurf Complex Targets Prickle 1 for Degradation

PCP proteins form discrete protein complexes that display asymmetric subcellular distribution patterns that function to establish and maintain tissue polarity (Strutt, 2002). Despite this, many PCP pathway components physically interact, raising puzzling questions about how asymmetry is achieved. Smurfs are E3 ligases that target proteins for localized degradation. Thus we investigated whether Smurfs might act to degrade specific PCP components and thereby contribute to the asymmetric distribution of PCP components. As Smurfs bind Dvls, we focused on PCP components that are known to display localization patterns opposite to Dvl, namely Vangl and Pk. We first determined that Smurf2 interacted with Pk1 and 2, but not Vangl1 or 2 (Figures 5A and S7D). Since Smurfs are recruited to Par6 via Dvl (Figure 4A) and Pk interacts with Dvl (Jenny et al., 2005), we considered whether Pk is a substrate of the Par6-phosphoDvl-Smurf complex. Examination of Pk interactions with Par6, revealed that Pk also associated with both wild-type Par6 and the Dvl-binding mutant, Par6 (Δ250–295) (Figure 5B). We next determined whether Pk1 bound to Par6 is subject to Smurf2-mediated degradation. Immunoprecipitation of Par6 and immunoblotting for associated Pk1 revealed that the levels of Pk1 bound to Par6 were decreased in the presence of Smurf2 WT, but not the catalytic mutant, Smurf2 CA (Figure 5C). Treatment with the proteasome inhibitor, LLnL also blocked Smurf2-mediated reduction in Pk1 protein. Importantly, wild-type Smurf2 had no effect on the levels of Pk1 bound to the Par6 Dvl-binding mutant (Δ250–295) (Figure 5C). To determine whether Pk1 ubiquitination is regulated by Smurf2, Pk1 bound to Par6 was isolated from LLnL-treated cells expressing HA-tagged ubiquitin, released under denaturing conditions, then subjected to anti-Flag immunoprecipitation followed by immunoblotting for ubiquitin-conjugated to Pk. Pk1 bound to Par6 was ubiquitinated in the presence of WT, but not CA,

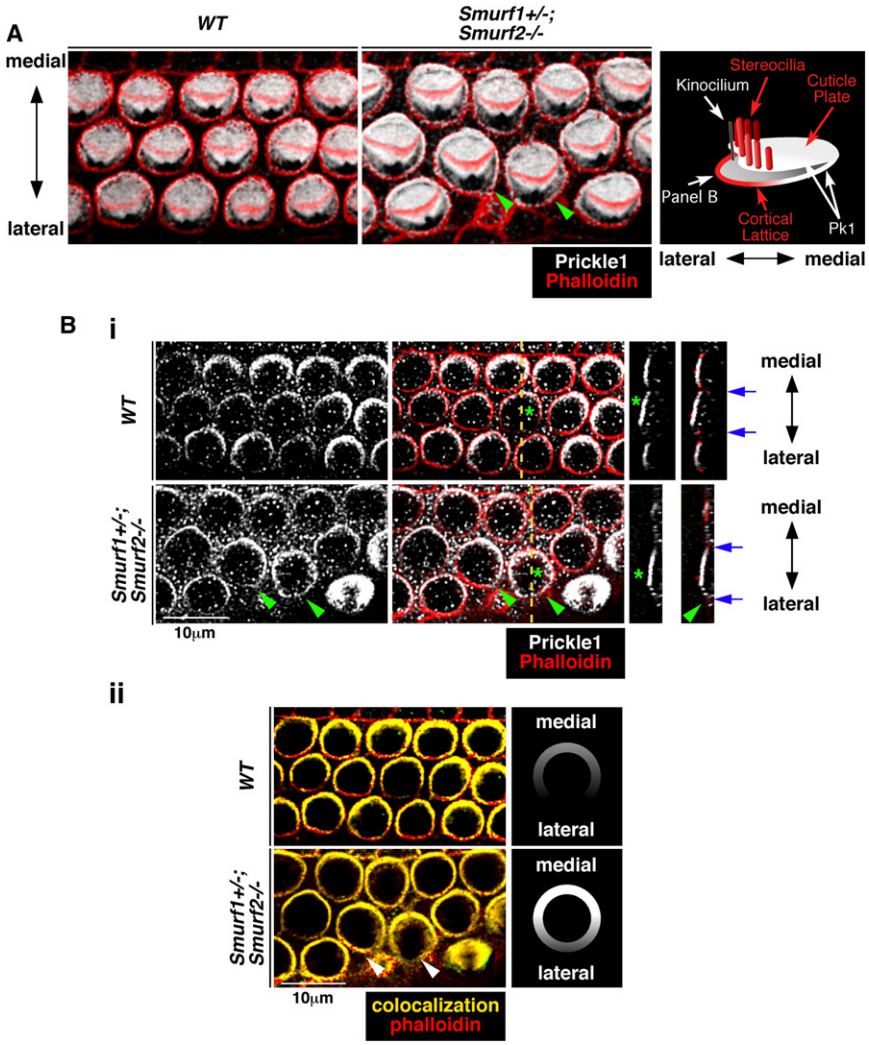

Figure 6. Alteration in the Mediolateral Gradient of Prickle1 in *Smurf* Mutant Cochlea

The cochlea from E18.5 wild-type and *Smurf1*$^{+/-}$; *Smurf2*$^{-/-}$ embryos were stained with anti-Prickle1 antibody (white) and TexasRed-phalloidin (red).

(A) 3D reconstructed images of the OHCs are shown. On the right is a schematic showing the organization of the apical aspect of the OHCs. In red are F-actin-rich structures that include the stereocilia, the cuticular plate rising to the apex of the cell and the cortical actin ring. The kinocilium (not detected in these stainings) is shown in gray. The observed Pk1 staining in a medial crescent on the cortical lattice and extending up into the cuticular plate is shown as white. Note the extensive colocalization of Pk1 and F-actin in medial structures in WT with expansion of Pk1 to the lateral side clearly visible in *Smurf* mutants.

(B) Optical sections of OHCs just below the cuticular plate are shown. Accumulation of Prickle1 at the lateral membrane of the sensory hair cells is observed in *Smurf1*$^{+/-}$;*Smurf2*$^{-/-}$ but not wild-type cochlea (arrowheads). Broken lines indicate positions of reconstructed cross sections (Bi, right). Blue arrows indicate the positions of lateral and medial membrane of indicated cells with asterisks. Note expansion of Pk1 to the lateral side of the OHCs (arrows). In Bii, membrane-localized Prickle1 was highlighted by visualizing the colocalization channel of Pk1 and F-actin. Pk1 colocalized with F-actin (yellow and red, respectively) extends laterally in the *Smurf* mutant OHCs.

Smurf2 or when bound to the Dvl binding mutant of Par6 (Figure 5D). These results demonstrate that Pk can bind Par6 and is subject to Dvl/Smurf-dependent ubiquitination and turnover.

Smurfs Are Required for Asymmetric Distribution of Prickle in the Cochlea and Floorplate

Our biochemical analyses indicated that Smurfs regulate Pk1 turnover, suggesting that Smurf is an effector of Dvl that regulates the asymmetric distribution of Pk1 by mediating localized targeting of Pk1 for ubiquitin-dependent degradation. To test whether Smurf is required for asymmetric distribution of Pk1, we first examined Pk1 protein localization in the organ of Corti using confocal microscopy and a Pk1-specific antibody (Figure S8). In wild-type cochlea, Pk1 strongly colocalized with F-actin in a crescent on the medial aspect of the cortical F-actin ring and extended apically into the F-actin-rich cuticular plate from which the stereocilia arise (Figure 6A). Of note, Pk1 did not stain the stereocilia. This is opposite to lateral Dvl2-EGFP previously observed in these cells (Wang et al., 2005) and is consistent with studies in *Drosophila*, where Pk and Dsh display asymmetric localization to opposite poles of the cell during establishment of PCP and recent analyses in the vestibule, where Pk2 displays asymmetric distribution in hair cells (Deans et al., 2007). However, in regions of the cochlea where compound *Smurf* mutants displayed disturbances in PCP, we observed expansion of Pk1 staining to the lateral surfaces of the cortical F-actin-rich lattice (Figure 6Bi). In particular, Pk1 colocalized with F-actin displayed a strong medial crescent in wild-type ears, whereas *Smurf* mutants exhibited Pk1 protein around the entire circumference of cortical F-actin (Figure 6Bii).

We then examined whether the loss of *Smurfs* in DKO mouse embryos affected Pk1 localization in the neurectoderm. In both control and *Smurf* DKO E8.0 embryos, Pk1 expression was detected in the neuroectoderm, as well as the notochord and endoderm (Figures 7A and S9). In control embryos, Pk1 was observed at the membrane in neuroectoderm cells and while Pk1 showed asymmetric distribution in individual neuroectoderm cells, at the multicellular level Pk1 displayed a variety of arrangements of asymmetry (Figure 7A). These results suggest that in the neural tube, asymmetric localization of Pk1 does not extend to the level of long-range tissue polarity that is typically observed in highly organized epithelial structures such as the mouse cochlear/vestibular hair cells and the *Drosophila* wing epithelium. The absence of long-range tissue polarity may reflect the highly

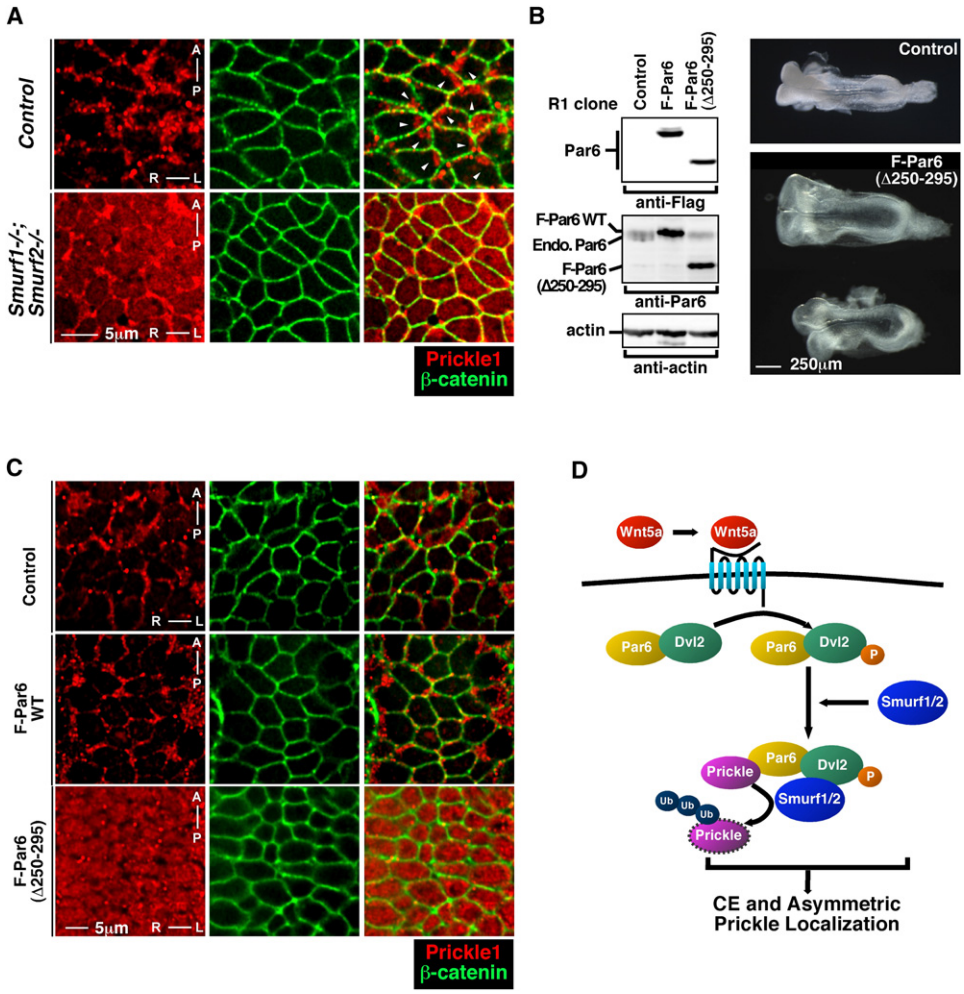

Figure 7. Altered Prickle1 Localization in the Floorplate of *Smurf1*$^{-/-}$;*Smurf2*$^{-/-}$ Mice

(A) Visualization of Prickle1 localization in the floorplate at E8.0. Optical sections of embryos immunostained with anti-Prickle1 and β-catenin antibodies are shown.

(B and C) Tetraploid embryos expressing a Par6 Dvl-binding mutant display CE defects and altered subcellular localization of Prickle1. An ES clone expressing Flag-Par6(Δ250-295) was subjected to aggregation with tetraploid embryos. (B) Dorsal view of a control and tetraploid chimera expressing Flag-Par6(Δ250–295) is shown. Immunoblotting of ES cell clone lysates confirmed expression of exogenous Par6. (C) Altered subcellular localization of Prickle1 in floorplate cells expressing Par6(Δ250-295). The chimeras at around E8.0 were immunostained with anti-Prickle1 and β-catenin antibodies and optical sections of the floorplate are shown. AP, DV, and RL axes are indicated.

(D) A model of localized Prickle degradation by the Par6-Dvl2-Smurf complex. Par6 interacts constitutively with Dvl2. Noncanonical Wnt binding leads to Dvl phosphorylation and membrane localization of the Dvl2-Par6 complex. Smurf is recruited by phosphorylated Dvl2 to Par6 and then locally ubiquitinates and degrades Par6-bound Prickle.

dynamic nature of the neuroectoderm at this stage of development. Regardless, the asymmetric distribution of Pk1 indicates that the molecular pathway of PCP signaling is active and that neuroectoderm cells possess planar asymmetry at a cellular level. In contrast, when we examined Pk1 in *Smurf* DKO embryos, we observed diffuse Pk1 localization and loss of the strong asymmetric distribution that was evident in wild-type embryos (Figure 7A). Furthermore, Pk1 protein levels measured by staining intensity were higher in *Smurf* DKO embryos (1.59 ± 0.06 fold over WT, n = 3). Thus Smurfs are required for the establishment of asymmetrically localized Pk1 in OHCs of the cochlea and in neuroectoderm cells at neurulation.

Pk1 bound to Par6 is targeted by Smurfs for ubiquitination and degradation in a Dvl-dependent manner. Therefore, we tested whether overexpression of Par6(Δ250–295), which fails to bind Dvl2 and protects Par6-bound Pk1 from Smurf ubiquitination (Figure 5), might interfere with PCP signaling in vivo. For this, mouse embryonic stem cells stably expressing wild-type Par6 and Par6(Δ250–295) were established and used to generate chimeric tetraploid embryos, in which ES cells contribute entirely to the embryo proper. Analysis at E8.5 revealed that Par6(Δ250–295) embryos displayed CE defects (Figure 7B) and that asymmetric Pk1 distribution was disturbed (Figure 7C), similar to *Smurf* DKO embryos. These results

indicate that ubiquitination/degradation of Pk1 mediated by Par6 and Smurf contributes to the asymmetric Pk1 localization in neuroectoderm cells during neurulation.

Altogether, these results establish Smurfs as key effectors of noncanonical Wnt signaling that function as effectors of a Par6/pDvl complex to promote the localized ubiquitination and degradation of Prickle. Localized targeting of Prickle for degradation would be an effective mechanism to establish and/or maintain the asymmetric distribution of Prickle during planar cell polarity signaling (Figure 7D).

DISCUSSION

PCP in vertebrates is regulated by noncanonical Wnt signaling and a set of core PCP pathway components that are conserved in *Drosophila*. Our results provide strong genetic and biochemical evidence that Smurf is a component of PCP signaling in mammals. In mice, partial or complete loss of Smurf1 and Smurf2 resulted in defects in CE and neural tube closure as well as disorganization of the cochlear hair cells, classic manifestations of the disruption of PCP. Interestingly, *Drosophila* possesses a Smurf homolog (Dsmurf) that regulates DPP signaling during early patterning (Podos et al., 2001). Whether Dsmurf functions in fly PCP pathways, where Wnt ligand is not required is unknown.

Mechanistic analysis of PCP signaling has revealed physical interactions between otherwise differentially localized PCP components that include interactions between Vangl, Prickle and Dvl (Bastock et al., 2003; Das et al., 2004; Jenny et al., 2005; Takeuchi et al., 2003; Torban et al., 2004; Tree et al., 2002). Here, we mapped interactions between Smurfs and components of the Wnt signaling pathway using a systematic screen and identified an interaction between Smurf and Dvl that is dependent on phosphorylation of Dvl. Accordingly, a DEP domain mutant that blocked Dvl phosphorylation also blocked Smurf interaction, as did a DEP mutation that is PCP-specific in the fly. These findings are in agreement with key roles previously defined for the DEP domain in PCP signaling in flies and vertebrates. We also identified constitutive interactions between Par6 and Dvl, consistent with previous observations in neurons (Zhang et al., 2007), as well as an interaction between Par6 and Prickle. Together, these results suggest a model in which Par6 is engaged in a trimeric complex with Prickle and Dvl that upon phosphorylation-dependent recruitment of Smurf to Dvl in response to Fzd signaling leads to Prickle ubiquitination and degradation (Figure 7D). Consistent with this, we found that Wnt5a induced Smurf-Par6 interactions and that Prickle bound to Par6 was subject to Smurf-dependent ubiquitination and turnover that was also dependent on the Dvl binding domain of Par6. Moreover, in *Smurf* mutants we observed increased levels of Pk1 protein, loss of the local asymmetric distribution of Pk1 in the neuroepithelium, and in the cochlea, Pk1 that was normally localized in a medial crescent in the OHCs, extended to the lateral side.

Dvl has also been shown to interact with the transmembrane protein Vangl, which also binds Pk (Torban et al., 2004) and Pk can antagonize Dvl function (Jenny et al., 2005). Moreover, Diego, an ankyrin repeat containing protein has been shown to directly compete with Pk for Dvl binding (Jenny et al., 2005) and can promote Dvl function in the PCP pathway via recruitment to membranes (Wu et al., 2008). Whether Diego functions primarily on Dvl, or plays a role in antagonizing Pk coassembled with Par6, perhaps in cooperation with Smurfs is unknown, but altogether these findings suggest that Pk and Dvl assemble via unique signaling complexes that respond to different extrinsic cues during PCP signaling. Consequently, while all PCP components might physically interact with each other, their asymmetric distribution may be maintained through dynamic modulation of complex membership.

Although PCP and CE have been linked via shared components and a key role for noncanonical Wnt signaling, the relationship of the molecular pathways governing tissue polarity to CE has been less clear. In particular, during CE the neuroepithelium and the underlying axial mesoderm do not display the highly organized structures typically associated with PCP and tissue polarity (Copp et al., 2003) and while Vangl and Dvl show asymmetric distribution in the cochlea (Montcouquiol et al., 2003; Wang et al., 2006a), there is no evidence for asymmetric distribution of either protein during CE in the mouse. Regardless, we clearly detected Par6-dependent asymmetric localization of endogenous Pk1 in neuroepithelial cells that was manifest at the cellular level, and in *Smurf* DKO mutants this asymmetry was lost. Furthermore, Par6 can also control the stable mediolateral extension of cell protrusions during CE (Hyodo-Miura et al., 2006). Localized Fzd signaling may thus regulate the asymmetric distribution of specific PCP components such as Pk1 in the absence of asymmetric distribution of *all* PCP pathway components. Vertebrates may thus broadly employ PCP signaling to control polarity at the local and even cellular level. Consistent with this, noncanonical Wnt signaling, Dvl and Par6 have all been shown to play key roles in regulating directed cell motility (Schlessinger et al., 2007) and the polarity of neurons (Zhang et al., 2007).

Our results demonstrate a noncanonical Wnt signaling pathway in which Smurf is recruited to Par6 via Dvl to regulate the degradation of PCP pathway components that in turn controls the asymmetric distribution of Pk1. Signal dependent degradation of PCP components may thus allow for dynamic use of the pathway in a local manner during convergent extension, as well as in the establishment of tissue polarity in organized epithelia such as the inner ear.

EXPERIMENTAL PROCEDURES

Generation of *Smurf1* and *Smurf2* Mutant Alleles and Tetraploid Chimeras

Gene targeting for *Smurf1* and *Smurf2* alleles was performed using R1 embryonic stem (ES) cells using standard procedures (see Supplemental Data). Chimeric mice were generated by diploid aggregation of ES cells and ICR embryos and heterozygous F1 mice harboring a targeted *Smurf1* or *Smurf2* allele were obtained by crossing chimeric males with ICR females. Wild-type and single heterozygotes, which do not show any phenotypic difference, were used as controls. For tetraploid chimeras, cell clones derived from R1 ES cells stably-expressing empty vector (pCAGIP), wild-type or mutant (Δ250–295) Flag-Par6C were aggregated with EGFP or RFP transgenic tetraploid embryos. Embryos with complete contribution of ES cells as assessed by fluorescence microscopy were selected.

In Situ Hybridization, Immunostaining, and Confocal Microscopy

For whole mount in situ hybridyzation and immunostaining, embryos were fixed in 4% paraformaldehyde in phosphate buffered saline (PBS), dehydrated with methanol and stored at −20°C. The organ of Corti was not dehydrated with methanol. In situ hybridization using digoxigenin-labeled probes and whole mount immunostaining were as described previously (Silvestri et al., 2008) using 10% donor bovine serum for blocking. Details of antibodies and counterstains are described in Supplementary Materials. For confocal imaging of the floor plate/notochord at E8.0, immunostained embryos were cleared in benzyl alcohol/benzyl benzoate (BABB) and scanned from the ventral side. All imaging and image analysis was performed using Volocity software (Improvision) with instrumentation and objectives as detailed in Supplementary Materials.

DNA Constructs and Production of Wnt5A

Tagged and mutant constructs subcloned into pCMV5B were generated by PCR or have been previously described (Barrios-Rodiles et al., 2005; Ozdamar et al., 2005; Wang et al., 2003). Wnt5A conditioned medium was collected from control or Wnt5A-expressing L cells (ATCC) cultured at confluence for 3 days in DMEM with 0.2% fetal bovine serum, centrifuged to remove cell debris, and stored at 4°C for up to 3 months.

Immunoprecipitation, Immunoblotting, and LUMIER

HEK293T cells were transiently-transfected with calcium-phosphate precipitation. Immunoprecipitation and immunoblotting were performed using commercially-available antibodies described in the Supplemental Data. For two-step immunoprecipitation, lysates were subjected to anti-Flag precipitation, eluted with Flag-peptide, and diluted 10-fold prior to anti-Myc immunoprecipitation. For phosphatase treatment, immunoprecipitates were washed, incubated with alkaline phosphatase (Fermentas) for 30 min at 37°C and then terminated by boiling. For LUMIER, Renilla Luciferase-tagged Smurf2 CA was assayed for interaction with Flag-tagged proteins by manual LUMIER (Barrios-Rodiles et al., 2005).

SUPPLEMENTAL DATA

Supplemental Data include Supplemental Experimental Procedures, Supplemental References, nine figures, and four tables and can be found with this article online at http://www.cell.com/supplemental/S0092-8674(09)00201-3.

ACKNOWLEDGMENTS

We thank Dr. W. Rod Hardy and the ES and transgenic core facilities at Samuel Lunenfeld Research Institute/Toronto Centre for Phenogenomics for supporting generation of ES clones and diploid/tetraploid chimeras. We thank Siyuan Song for technical assistance, Dr. H. McNeill and the members of Drs. Wrana's and Attisano's labs for helpful comments and discussion. This work was supported by grants to L.A. (#77690) and J.L.W. (#74692, #12860) from the Canadian Institutes of Health Research (CIHR). L.A. and J.L.W. hold Canadian Research Chairs, and J.L.W. is an International Scholar of the Howard Hughes Medical Institute.

Received: June 17, 2008
Revised: December 3, 2008
Accepted: February 10, 2009
Published: April 16, 2009

REFERENCES

Axelrod, J.D., Miller, J.R., Shulman, J.M., Moon, R.T., and Perrimon, N. (1998). Differential recruitment of Dishevelled provides signaling specificity in the planar cell polarity and Wingless signaling pathways. Genes Dev. *12*, 2610–2622.

Barrios-Rodiles, M., Brown, K.R., Ozdamar, B., Bose, R., Liu, Z., Donovan, R.S., Shinjo, F., Liu, Y., Dembowy, J., Taylor, I.W., et al. (2005). High-throughput mapping of a dynamic signaling network in mammalian cells. Science *307*, 1621–1625.

Bastock, R., Strutt, H., and Strutt, D. (2003). Strabismus is asymmetrically localised and binds to Prickle and Dishevelled during *Drosophila* planar polarity patterning. Development *130*, 3007–3014.

Boutros, M., Paricio, N., Strutt, D.I., and Mlodzik, M. (1998). Dishevelled activates JNK and discriminates between JNK pathways in planar polarity and wingless signaling. Cell *94*, 109–118.

Ciruna, B., Jenny, A., Lee, D., Mlodzik, M., and Schier, A.F. (2006). Planar cell polarity signalling couples cell division and morphogenesis during neurulation. Nature *439*, 220–224.

Classen, A.K., Anderson, K.I., Marois, E., and Eaton, S. (2005). Hexagonal packing of *Drosophila* wing epithelial cells by the planar cell polarity pathway. Dev. Cell *9*, 805–817.

Copp, A.J., Greene, N.D., and Murdoch, J.N. (2003). The genetic basis of mammalian neurulation. Nature reviews *4*, 784–793.

Curtin, J.A., Quint, E., Tsipouri, V., Arkell, R.M., Cattanach, B., Copp, A.J., Henderson, D.J., Spurr, N., Stanier, P., Fisher, E.M., et al. (2003). Mutation of Celsr1 disrupts planar polarity of inner ear hair cells and causes severe neural tube defects in the mouse. Curr. Biol. *13*, 1129–1133.

Das, G., Jenny, A., Klein, T.J., Eaton, S., and Mlodzik, M. (2004). Diego interacts with Prickle and Strabismus/Van Gogh to localize planar cell polarity complexes. Development *131*, 4467–4476.

Deans, M.R., Antic, D., Suyama, K., Scott, M.P., Axelrod, J.D., and Goodrich, L.V. (2007). Asymmetric distribution of prickle-like 2 reveals an early underlying polarization of vestibular sensory epithelia in the inner ear. J. Neurosci. *27*, 3139–3147.

Greene, N.D., Gerrelli, D., Van Straaten, H.W., and Copp, A.J. (1998). Abnormalities of floor plate, notochord and somite differentiation in the loop-tail (Lp) mouse: a model of severe neural tube defects. Mech. Dev. *73*, 59–72.

Hyodo-Miura, J., Yamamoto, T.S., Hyodo, A.C., Iemura, S., Kusakabe, M., Nishida, E., Natsume, T., and Ueno, N. (2006). XGAP, an ArfGAP, is required for polarized localization of PAR proteins and cell polarity in Xenopus gastrulation. Dev. Cell *11*, 69–79.

Izzi, L., and Attisano, L. (2006). Ubiquitin-dependent regulation of TGFbeta signaling in cancer. Neoplasia *8*, 677–688.

Jenny, A., Reynolds-Kenneally, J., Das, G., Burnett, M., and Mlodzik, M. (2005). Diego and Prickle regulate Frizzled planar cell polarity signalling by competing for Dishevelled binding. Nat. Cell Biol. *7*, 691–697.

Jiang, D., Munro, E.M., and Smith, W.C. (2005). Ascidian prickle regulates both mediolateral and anterior-posterior cell polarity of notochord cells. Curr. Biol. *15*, 79–85.

Keller, R. (2002). Shaping the vertebrate body plan by polarized embryonic cell movements. Science *298*, 1950–1954.

Kibar, Z., Vogan, K.J., Groulx, N., Justice, M.J., Underhill, D.A., and Gros, P. (2001). Ltap, a mammalian homolog of *Drosophila* Strabismus/Van Gogh, is altered in the mouse neural tube mutant Loop-tail. Nat. Genet. *28*, 251–255.

Lewis, J., and Davies, A. (2002). Planar cell polarity in the inner ear: how do hair cells acquire their oriented structure? J. Neurobiol. *53*, 190–201.

Montcouquiol, M., Rachel, R.A., Lanford, P.J., Copeland, N.G., Jenkins, N.A., and Kelley, M.W. (2003). Identification of Vangl2 and Scrb1 as planar polarity genes in mammals. Nature *423*, 173–177.

Montcouquiol, M., Sans, N., Huss, D., Kach, J., Dickman, J.D., Forge, A., Rachel, R.A., Copeland, N.G., Jenkins, N.A., Bogani, D., et al. (2006). Asymmetric localization of Vangl2 and Fz3 indicate novel mechanisms for planar cell polarity in mammals. J. Neurosci. *26*, 5265–5275.

Murdoch, J.N., Doudney, K., Paternotte, C., Copp, A.J., and Stanier, P. (2001). Severe neural tube defects in the loop-tail mouse result from mutation of Lpp1, a novel gene involved in floor plate specification. Hum. Mol. Genet. *10*, 2593–2601.

Ogunjimi, A.A., Briant, D.J., Pece-Barbara, N., Le Roy, C., Di Guglielmo, G.M., Kavsak, P., Rasmussen, R.K., Seet, B.T., Sicheri, F., and Wrana, J.L. (2005).

Regulation of Smurf2 ubiquitin ligase activity by anchoring the E2 to the HECT domain. Mol. Cell *19*, 297–308.

Ozdamar, B., Bose, R., Barrios-Rodiles, M., Wang, H.R., Zhang, Y., and Wrana, J.L. (2005). Regulation of the polarity protein Par6 by TGFbeta receptors controls epithelial cell plasticity. Science *307*, 1603–1609.

Penton, A., Wodarz, A., and Nusse, R. (2002). A mutational analysis of dishevelled in *Drosophila* defines novel domains in the dishevelled protein as well as novel suppressing alleles of axin. Genetics *161*, 747–762.

Podos, S.D., Hanson, K.K., Wang, Y.C., and Ferguson, E.L. (2001). The DSmurf ubiquitin-protein ligase restricts BMP signaling spatially and temporally during *Drosophila* embryogenesis. Dev. Cell *1*, 567–578.

Qian, D., Jones, C., Rzadzinska, A., Mark, S., Zhang, X., Steel, K.P., Dai, X., and Chen, P. (2007). Wnt5a functions in planar cell polarity regulation in mice. Dev. Biol. *306*, 121–133.

Sahai, E., Garcia-Medina, R., Pouyssegur, J., and Vial, E. (2007). Smurf1 regulates tumor cell plasticity and motility through degradation of RhoA leading to localized inhibition of contractility. J. Cell Biol. *176*, 35–42.

Schlessinger, K., McManus, E.J., and Hall, A. (2007). Cdc42 and noncanonical Wnt signal transduction pathways cooperate to promote cell polarity. J. Cell Biol. *178*, 355–361.

Seifert, J.R., and Mlodzik, M. (2007). Frizzled/PCP signalling: a conserved mechanism regulating cell polarity and directed motility. Nature reviews *8*, 126–138.

Silvestri, C., Narimatsu, M., von Both, I., Liu, Y., Tan, N.B., Izzi, L., McCaffery, P., Wrana, J.L., and Attisano, L. (2008). Genome-wide identification of Smad/Foxh1 targets reveals a role for Foxh1 in retinoic acid regulation and forebrain development. Dev. Cell *14*, 411–423.

Strutt, D.I. (2002). The asymmetric subcellular localisation of components of the planar polarity pathway. Semin. Cell Dev. Biol. *13*, 225–231.

Takeuchi, M., Nakabayashi, J., Sakaguchi, T., Yamamoto, T.S., Takahashi, H., Takeda, H., and Ueno, N. (2003). The prickle-related gene in vertebrates is essential for gastrulation cell movements. Curr. Biol. *13*, 674–679.

Torban, E., Wang, H.J., Groulx, N., and Gros, P. (2004). Independent mutations in mouse Vangl2 that cause neural tube defects in looptail mice impair interaction with members of the Dishevelled family. J. Biol. Chem. *279*, 52703–52713.

Tree, D.R., Shulman, J.M., Rousset, R., Scott, M.P., Gubb, D., and Axelrod, J.D. (2002). Prickle mediates feedback amplification to generate asymmetric planar cell polarity signaling. Cell *109*, 371–381.

Wallingford, J.B., Fraser, S.E., and Harland, R.M. (2002). Convergent extension: the molecular control of polarized cell movement during embryonic development. Dev. Cell *2*, 695–706.

Wang, H.R., Zhang, Y., Ozdamar, B., Ogunjimi, A.A., Alexandrova, E., Thomsen, G.H., and Wrana, J.L. (2003). Regulation of cell polarity and protrusion formation by targeting RhoA for degradation. Science *302*, 1775–1779.

Wang, J., Hamblet, N.S., Mark, S., Dickinson, M.E., Brinkman, B.C., Segil, N., Fraser, S.E., Chen, P., Wallingford, J.B., and Wynshaw-Boris, A. (2006a). Dishevelled genes mediate a conserved mammalian PCP pathway to regulate convergent extension during neurulation. Development *133*, 1767–1778.

Wang, J., Mark, S., Zhang, X., Qian, D., Yoo, S.J., Radde-Gallwitz, K., Zhang, Y., Lin, X., Collazo, A., Wynshaw-Boris, A., et al. (2005). Regulation of polarized extension and planar cell polarity in the cochlea by the vertebrate PCP pathway. Nat. Genet. *37*, 980–985.

Wang, Y., Guo, N., and Nathans, J. (2006b). The role of Frizzled3 and Frizzled6 in neural tube closure and in the planar polarity of inner-ear sensory hair cells. J. Neurosci. *26*, 2147–2156.

Wang, Y., and Nathans, J. (2007). Tissue/planar cell polarity in vertebrates: new insights and new questions. Development *134*, 647–658.

Wu, J., Jenny, A., Mirkovic, I., and Mlodzik, M. (2008). Frizzled-Dishevelled signaling specificity outcome can be modulated by Diego in *Drosophila*. Mech. Dev. *125*, 30–42.

Yamashita, M., Ying, S.X., Zhang, G.M., Li, C., Cheng, S.Y., Deng, C.X., and Zhang, Y.E. (2005). Ubiquitin ligase Smurf1 controls osteoblast activity and bone homeostasis by targeting MEKK2 for degradation. Cell *121*, 101–113.

Ybot-Gonzalez, P., Gaston-Massuet, C., Girdler, G., Klingensmith, J., Arkell, R., Greene, N.D., and Copp, A.J. (2007). Neural plate morphogenesis during mouse neurulation is regulated by antagonism of Bmp signalling. Development *134*, 3203–3211.

Zallen, J.A. (2007). Planar polarity and tissue morphogenesis. Cell *129*, 1051–1063.

Zhang, X., Zhu, J., Yang, G.Y., Wang, Q.J., Qian, L., Chen, Y.M., Chen, F., Tao, Y., Hu, H.S., Wang, T., et al. (2007). Dishevelled promotes axon differentiation by regulating atypical protein kinase C. Nat. Cell Biol. *9*, 743–754.